Journal of the European Ceramic Society xxx (2016) xxx–xxx

Contents lists available at www.sciencedirect.com

Journal of the European Ceramic Society

journal homepage: www.elsevier.com/locate/jeurceramsoc

# Dielectric and energy storage properties of Mn-doped $Ba_{0.3}Sr_{0.475}La_{0.12}Ce_{0.03}TiO_3$ dielectric ceramics

X.Y. Ye, Y.M. Li, J.J. Bian*

*Department of Inorganic Materials, Shanghai University, 333 Nanchen Road, Shanghai 200444, China*

ARTICLE INFO

*Article history:*
Received 5 February 2016
Received in revised form 1 August 2016
Accepted 4 August 2016
Available online xxx

*Keywords:*
BST
Mn-doping
Dielectric properties
Energy storage properties

ABSTRACT

Microstructure, temperature and frequency dependent dielectric and energy storage properties of $Ba_{0.3}Sr_{0.475}La_{0.12}Ce_{0.03}Ti_{1-x}Mn_xO_3(x=0-0.005)$ have been investigated with X-ray diffractometer, and scanning electron microscope, broad band dielectric spectrometer and ferroelectric analyzer. The doping of Mn substantially decreased the dielectric loss, but made some of $Ce^{3+}$ be oxidized to $Ce^{4+}$ entering into B-site, which resulted in the formation secondary phases. For the Mn-doped composition, extremely low dielectric loss ($10^{-5}$ order of magnitude at 10 kHz) could be obtained at room temperature. The relaxation mechanism at low temperature is of the dipole type for the undoped composition and that at high temperature (>500 K) is governed by the trap controlled ac conduction, respectively. The energy storage properties were improved by the doping with Mn due to the increase of insulation. Maximum energy density of 0.953 J/cm$^3$ could be obtained for x = 0.003 composition with the BDS of 247 kV/cm and efficiency of 93%.



## 1. Introduction

Energy storage in dielectrics received much attention as the increasing demand of compact electronics. Dielectric capacitors are key energy storage components in pulse power circuit due to its higher power density compared with other energy storage materials [1–4]. The energy storage density J in dielectric ceramic can be described as $J = \int_{E1}^{E2} PdE$, where J is the energy storage density (J/cm$^3$), E is the applied electric filed and P is the polarization induced in the dielectric by the applied field [5]. The highest recoverable energy density increases with the increase in dielectric permittivity and breakdown field strength. Several factors such as porosity, grain size, defects, temperature and presence of secondary phase, etc affect the break down strength (BDS) of the ceramic. High density, small grain size, low concentration of defects and presence of secondary phase with high breakdown strength such as glass is usually helpful to increase the BDS. The sample thickness or even electrode area also remarkably influence the BDS [6,7]. It generally increases with the decrease in sample thickness. Since the detail measurement condition for BDS was not provided in most references, it's difficult to compare the data of BDS values reported by different references.

Various dielectric ceramics have been investigated for high energy density applications. They can be usually divided into three categories: ferroelectrics, antiferroelectrics and linear dielectrics. Although ferroelectric ceramics usually have high dielectric permittivity, the recoverable energy storage densities are limited due to the combination of field-induced stiffening of the dielectric response, the lower dielectric breakdown strength in ceramics and the energy loss from the hysteresis [8]. Love et al. [1], considered that maximum energy storage is not obtained in high dielectric constant materials but in those materials which display intermediate dielectric constant and highest ultimate breakdown voltage. Fletcher et al. [9], presented a theoretical treatment, based on the Devonshire theory of ferroelectrics, to describe the storage of electrostatic energy in ferroelectric and paraelectric materials at very high field strengths. In all cases, they found that optimal energy density is achieved by using compositions with Curie temperatures well below the operating temperature. Barium titanium based materials dominated most of the ferroelectric and linear dielectric capacitors reported. For example, Liu et al. [10] prepared fine-crystalline $BaTiO_3$ ceramics by coating powders with 3 wt% of $Al_2O_3$ and 1 wt% of $SiO_2$, the energy storage density was 0.725 J/cm$^3$ and the efficiency could maintain above 80%, the dielectric breakdown strength was 190 kV/cm. High dielectric breakdown strength of 300 kV/cm, maximum energy storage density of 1.50 J/cm$^3$ and high

* Corresponding author.
*E-mail address:* jjbian@shu.edu.cn (J.J. Bian).

http://dx.doi.org/10.1016/j.jeurceramsoc.2016.08.002
0955-2219/

Please cite this article in press as: X.Y. Ye, et al., Dielectric and energy storage properties of Mn-doped $Ba_{0.3}Sr_{0.475}$ $La_{0.12}Ce_{0.03}TiO_3$ dielectric ceramics, *J Eur Ceram Soc* (2016), http://dx.doi.org/10.1016/j.jeurceramsoc.2016.08.002

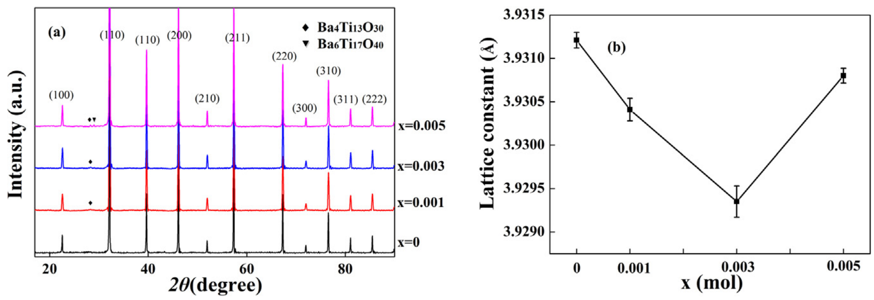

**Fig. 1.** (a) Powder XRD patterns and (b) variation of lattice parameter with Mn-doping concentration for $Ba_{0.3}Sr_{0.475}La_{0.12}Ce_{0.03}Ti_{1-x}Mn_xO_3$ ceramics.

energy storage efficiency of 88.5% were obtained in the dense and fine-crystalline $Ba_{0.4}Sr_{0.6}TiO_3$-MgO composite prepared by spark plasma sintering (SPS) method [11]. Recently, 0.7$BaTiO_3$–0.3$BiScO_3$ ceramic thick film (15 μm) was found to have energy density of about 6.1 J/cm$^3$ at a field of 73 kV/mm at room temperature, which is temperature stable up to 300 °C. However its dielectric loss is relatively high (tan$\delta$ = 0.15 @10 kHz), which limited its energy storage efficiency [8].

Based on the above consideration, we focused on the improvement of dielectric loss and temperature stability of BST based ceramic as well as retaining its high energy storage density in this work. Rare earth cations doping on A-site were reported to shift the Tc toward lower temperature and decrease the dielectric loss of BST ceramic [12–14]. In this paper, therefore, we adopted the $La^{3+}$ and $Ce^{3+}$ co-doping on A-site. In order to further decrease the dielectric loss caused by the possible reduction of $Ti^{4+}$, the composition was doped with different concentration of Mn on B-site. The temperature and frequency dependent dielectric properties and energy storage properties of the $Ba_{0.3}Sr_{0.475}Ce_{0.03}La_{0.12}Ti_{1-x}Mn_xO_3$ ceramics have been investigated in this paper.

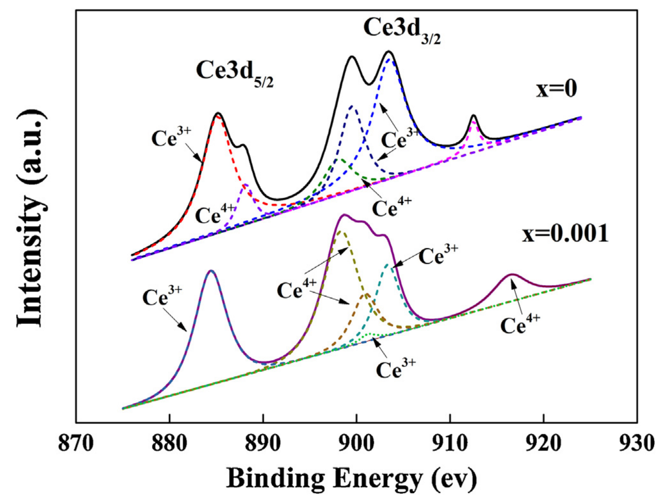

**Fig. 2.** XPS spectra for Ce 3d (left) of x = 0 and 0.001compositions.

## 2. Experimental

$Ba_{0.3}Sr_{0.475}La_{0.12}Ce_{0.03}Ti_{1-x}Mn_xO_3$ (x = 0 – 0.005) were prepared by traditional solid-state reaction process. $BaCO_3$ (99.7%), $SrCO_3$ (99.5%), $TiO_2$ (99.7%), $CeO_2$ (99.9%), $La_2O_3$ (99.9%) and $MnO_2$ (99.95%) powders were used as the starting materials. The starting powders were weighed according to the above formula and then mixed in poly-propylene bottle with zirconia grinding media in deionized water for 24 h; then the dried powders were calcined at 1200 °C for 2 h in air. The calcined powders were again wet ground for 24 h, after that the dried calcined powders were mixed with 7–10 wt% PVA as binder and granulated. The granulated powders were uni-axially pressed into pellets with 10 mm in diameter and 1–4.5 mm in height under the pressure of 100 Mpa. The pellets were sintered at the temperatures in the range from 1250 °C to 1350 °C for 2 h. Some of the compositions were sintered under the $O_2$ atmosphere at the same temperature for comparison.

X-ray powder diffraction (XRD) with Ni-filtered CuKα radiation (Model Dmax-RC, Japan) was utilized to characterize the phase identification. The microstructure of the sintered sample was characterized by scanning electron microscopy (SEM) (Model JSM-6700F, JEOL, Tokyo, Japan). The samples for the back scattering SEM were polished without thermal etching, and those for secondary electron SEM were polished thermal etched at the temperature of 70–100 °C lower than its sintering temperature for 30 min. The valence states of Ti and Ce were detected by X-ray photoelectron spectroscopy (Model ESCALAB 250 Xi, England).

Low frequency (1 kHz–1 MHz) dielectric properties measurements were performed on 1 mm thick samples using a Broadband Dielectric Spectrometer (Model Novocontrol Germany). Silver paste containing small amount of $B_2O_3$-$Bi_2O_3$ glass frit were used to coat electrodes on both polished surfaces of the sample by screen printing method and fired at 840 °C for 12 min to form a metal–insulator–metal capacitor for electrical test. Temperature dependences of permittivity and loss tangent were measured over different frequencies from 1 kHz to 1 MHz and temperatures from 123 K to 900 K. P-E loops and BDS measurements were performed on 0.1–0.2 mm thick samples in silicon oil at the frequency of 10 Hz and room temperature with internal bias voltages up to 4000 V by Ferroelectric analyzer (Model TF analyzer 2000E, aix ACCT system, Germany). Microwave dielectric properties of the sintered samples were measured at about 3 GHz using network analyzer (Hewlett Packard, Model HP8720C, USA). The quality factor was measured by the transmission cavity method using the pellet with 8.5 mm in diameter and 3.5 mm high. The cylindrical cavity has the same aspect ratio as the sample and a ratio of the cavity diameter over the sample diameter about 3.2. $TE_{01\delta}$ resonant mode was adopted. The dielectric permittivity was measured according to the Hakki–Coleman method using the $TE_{011}$ resonant mode.

## 3. Results and discussion

Fig. 1(a) shows powder XRD patterns of the sintered samples doped with different level of Mn. The undoped specimen demonstrates single perovskite phase (Pm-3m), while the Mn-doped ones exhibit trace amount of secondary phases including $Ba_4Ti_{13}O_{30}$ (JCPDS# 35-0750) and $Ba_6Ti_{17}O_5$ (JCPDS# 26-0321), which increase with the increase in doping concentration. The appearance of $Ba_4Ti_{13}O_{30}$ and $Ba_6Ti_{17}O_5$ secondary phases with Mn dopant can be attributed to the variation of valence state of Ce as evidenced by XPS analysis shown in Fig. 2 and Table 1. Some of the Ce occupying A-site would enter into B-site as result of the oxidization of